AIP Journal of Applied Physics

Least-squares analysis of x-ray diffraction line shapes with analytic functions

C. R. Houska and Terence M. Smith

Citation: Journal of Applied Physics 52, 748 (1981); doi: 10.1063/1.328757
View online: http://dx.doi.org/10.1063/1.328757
View Table of Contents: http://scitation.aip.org/content/aip/journal/jap/52/2?ver=pdfcov
Published by the AIP Publishing

Articles you may be interested in

Least-squares fit analysis program for the evaluation of spatially resolved x-ray spectra from tokamak plasmas
Rev. Sci. Instrum. **75**, 3756 (2004); 10.1063/1.1790045

Deblurring of x-ray spectra acquired with a NaI-photomultiplier detector by constrained least-squares deconvolution
Med. Phys. **29**, 787 (2002); 10.1118/1.1469628

Coded-aperture x- or γ -ray telescope with least-squares image reconstruction. III. Data acquisition and analysis enhancements
Rev. Sci. Instrum. **68**, 2404 (1997); 10.1063/1.1148124

Linearized least-squares data analysis
J. Acoust. Soc. Am. **94**, 1855 (1993); 10.1121/1.407663

Summary Abstract: Nonlinear least-squares fitting employing fast Fourier transform background generation for the x-ray photoelectron spectroscopy analysis of iron oxidation
J. Vac. Sci. Technol. A **6**, 1044 (1988); 10.1116/1.575631

MIT LINCOLN LABORATORY CAREERS
Discover the satisfaction of innovation and service to the nation
Space Control
Air & Missile Defense
Communications Systems & Cyber Security
Intelligence, Surveillance and Reconnaissance Systems
Advanced Electronics
Tactical Systems
Homeland Protection
Air Traffic Control

[This article is copyrighted as indicated in the article. Reuse of AIP content is subject to the terms at: http://scitation.aip.org/termsconditions. Downloaded to] IP: 128.173.126.47 On: Wed, 06 May 2015 21:25:18

Least-squares analysis of x-ray diffraction line shapes with analytic functions

C. R. Houska
Department of Materials Engineering, Virginia Polytechnic Institute and State University, Blacksburg, Virginia 24061

Terence M. Smith
Tektronix Laboratory, P.O. Box 500, Beaverton, Oregon 97077

(Received 11 August 1980; accepted for publication 17 October 1980)

This is a second paper of a sequence that provides a useful analytic function which is based upon the Warren-Averbach line shape analysis. Once the Fourier coefficients are interrelated in terms of a minimum number of parameters, the rather lengthy Fourier series can be evaluated by reducing it to a convolution of two known functions. One of these functions includes the particle size distribution, strain, and the Cauchy-like contribution to the instrumental broadening. The second includes another strain parameter and the Gaussian contribution to the instrumental broadening. The resultant convolution integral is readily carried out using a nine-point Gauss-Legendre quadrature. Instrumental parameters are obtained from a separate convolution of Cauchy and Gaussian functions. This procedure reduces the computer time to one-tenth the time required to synthesize the Fourier series and makes it feasible to carry out a least-squares fitting of the profile data. Examples are given for Mo films and for an InSb film.

PACS numbers: 61.70. − r, 61.80.Cb

INTRODUCTION

In a previous paper,[1] it was demonstrated that the Fourier coefficients in the Warren-Averbach line shape analysis[2] can be interrelated with five parameters for two orders. They include two strain parameters that describe the falloff of nonuniform microstrain with increasing distance, the average particle size, an instrumental parameter for each order, and an intensity scaling factor for each order. The instrumental parameters are obtained separately by fitting a Cauchy profile to data obtained from ideal samples giving only instrumental broadening. Consequently, the total number of parameters used to fit "n" specimen broadened multiple order profiles is $3 + n$. The present paper extends the previous one by giving an analytical expression that reduces computer time to about one-tenth of our previous approach. Also, the requirement that the instrumental broadening must be of a pure Cauchy form has been eliminated.

The new analysis provides useful data even though entire profiles are not available. The classical Warren-Averbach analysis gives a hook effect when for one reason or another the full profile is not measurable. This may introduce considerable error in the results. Examples are given that demonstrate the effect of truncating the number of data points in the peak tails and also the effect of using only one-half of each profile. A 50% truncation still gives acceptable values for all parameters while 75% truncation gives strain parameters that are still quite good but a particle size that is too low.

The new analytical function can be generated quickly enough to make use of nonlinear least-squares fitting routines. By intentionally selecting particle and strain parameters away from the optimum point, error plots can be obtained that show the sharpness of the least-squares fit. A broad error surface would provide a range of strain or particle size parameters and a low confidence level for any single set. Whereas, one that is sharp along a specific parameter axis would represent a high level of confidence in that parameter. Similar surfaces can be generated from the instrumental profiles. This kind of interpretation is not feasible with the classical analysis and becomes especially important when only one peak is used to obtain strain and particle size information.

THEORY

The shape of a diffraction line can be described by[2]

$$P'(h_3) = Y_o\left\{1 + 2\sum_{n=1}^{\infty} A_n \cos[2\pi n(h_3 - l)]\right\}, \qquad (1)$$

where h_3 is the usual reciprocal space variable given by $h_3 = 2\langle d\rangle \sin\theta/\lambda$, $\langle d\rangle$ is the average interplanar spacing for $(00l)$ planes, θ is the angle of incidence, and λ is the wavelength. Y_o is considered to be a constant for a reflection. The Fourier coefficient A_n is defined as a product of coefficients. Individual coefficients contain information about the degree of perfection of the specimen, as well as broadening from the instrument. The latter includes the broadening effect from the spectral distribution of wavelengths that are counted from the detector. In order to have the option of working with incomplete profiles, the strain and particle size coefficients were interrelated for different n values by three parameters.[1] In this paper, one additional parameter is included to better describe the shape of the instrument broadening.

The Fourier coefficient in Eq. (1) can be written in two ways that are experimentally indistinguishable. These are given by

$$A_n = (A^I_C)^n (A^I_G)^{n^2} A^S_n (A^D_{1F})^{n^q} \qquad (2a)$$

$$A_n = (A^I_C)^n (A^I_G)^{n^2} A^S_n (A^D_1)^n (A^U_1)^{n^2}. \qquad (2b)$$

In the following discussion, a brief description is given of the individual Fourier coefficients. The strain coefficient can be written as

 0021-8979/81/020748-07$01.10 © 1981 American Institute of Physics

[This article is copyrighted as indicated in the article. Reuse of AIP content is subject to the terms at: http://scitation.aip.org/termsconditions. Downloaded to] IP: 128.173.126.47 On: Wed, 06 May 2015 21:25:18

$$(A_{1F}^{D})^{n^q} = [\exp(-2\pi^2 <\epsilon_1^2> l^2)]^{n^q}, \quad (3)$$

where $q = 2(r+1)$ and r allows the total n^{th} neighbor strain to be related to the first according to

$$<\epsilon_n^2>^{1/2} = |n|^r <\epsilon_1^2>^{1/2}. \quad (4)$$

The restriction $-1/2 \leqslant r \leqslant 0$ is imposed[1] with $r = -1/2$ taken to represent the strains associated with a dislocation network.[3] The second definition of the strain coefficient is given as a product of the individual terms corresponding to the two extreme strain distributions found in certain sputtered films,

$$(A_1^D)^n = [\exp(-2\pi^2 \langle \epsilon_{1D}^2 \rangle l^2)]^n \quad r = -1/2, \quad (5a)$$

$$(A_1^U)^{n^2} = [\exp(-2\pi^2 \langle \epsilon_{1U}^2 \rangle l^2)]^{n^2} \quad r = 0, \quad (5b)$$

where the mean-square strain $\langle \epsilon_{1D}^2 \rangle$ is relatable to pure dislocation sources and $\langle \epsilon_{1U}^2 \rangle$ has been associated with atoms becoming embedded in films during the sputtering process.[4] The alternate expressions [Eqs. (5a) and (5b)] can be obtained by convoluting the strain distributions associated with these defects. The strain field giving $\langle \epsilon_{1u}^2 \rangle$ and the related broadening requires the special constraints found in film specimens with only one surface free to move. It could be set equal to zero for more conventional studies of cold-worked metals having point defects in solids with unconstrained free surfaces.

The particle size coefficient is given by

$$A_n^S = 1 - \frac{n}{N_3} + \frac{4}{27}\left(\frac{n}{N_3}\right)^3, \quad n < \frac{3}{2}N_3, \quad (6a)$$

$$A_n^S = 0, \quad n \geqslant \frac{3}{2}N_3, \quad (6b)$$

where N_3 is the average number of unit cells per column. The first two terms in Eq. (6a) represent the fraction of nth neighbors for columns of the same height. The cubic term allows for the distribution of heights within an entire sample. In the present case, it has been approximated by the column length distribution of a sphere.

The first of the instrumental coefficients is relatable to the Cauchy-like character of the instrumental broadening and is defined by

$$A_C^I = \exp(-2\pi a_\gamma), \quad (7)$$

where a_γ representing a shape fitting parameter. This coefficient is obtained by taking the Fourier transform of the normalized Cauchy function, i.e.,

$$g_1(h_3) = (1/\pi a_\gamma)(1 + h_3^2/a_\gamma^2)^{-1}, \quad (8)$$

while

$$A_G^I = \exp(-\pi a_\beta^2), \quad (9)$$

is obtained from the Fourier transform of a normalized Gaussian function given by

$$g_2(h_3) = (1/a_\beta)\exp(-\pi h_3^2/a_\beta^2). \quad (10)$$

It is well known that when Fourier coefficients are multiplied, this is equivalent to convoluting the original functions from which the coefficients were derived.[5] Equation (1) can be interpreted in this sense. One can begin with an ideal sample giving very sharp reflection points described by delta functions. If one introduces internal boundaries, the reflections become broadened and this can be introduced by convoluting the delta function with the appropriate particle size function. Likewise, the effect of dislocation strain fields or other strain distributions that produce broadening can be introduced by successive convolutions. This is imagined as a systematic and independent process of introducing various defects that give special broadening affects. In the case of strain broadening, one can introduce a single strain distribution as given by Eq. (4) or convolute with two extreme distributions having $r = -\frac{1}{2}$ and $r = 0$. Both approaches given an equally good fit. If one begins with the latter approach, r and $<\epsilon_1^2>$ can be determined from a best fit of

$$(1/n)\langle \epsilon_{1D}^2 \rangle + \langle \epsilon_{1U}^2 \rangle = n^{2r} \langle \epsilon_1^2 \rangle = \langle \epsilon_n^2 \rangle. \quad (11)$$

Equation (1) is cumbersome to use as a Fourier series having many terms and can be put into a much more useful form for computer calculations. This sum is best carried out as an equivalent integration. The following definitions are required to change variables and to simplify the equations:

$$u = n/N_3, h_3^0 = N_3 h_3 \quad (12)$$

and

$$\gamma = 2\pi N_3(a_\gamma + \pi <\epsilon_{1D}^2> l^2), \quad (13a)$$

$$\beta = \pi N_3^2(a_\beta^2 + 2\pi <\epsilon_{1U}^2> l^2). \quad (13b)$$

This enables one to write the integral

$$\frac{P'(h_3^0)}{2N_3 Y_0} = \int_0^{3/2} \left(1 - u + \frac{4}{27}u^3\right) e^{-(\gamma u + \beta u^2)} \cos 2\pi h_3^0 u \, du. \quad (14)$$

A useful result can be obtained by setting $\beta = 0$ and evaluating the sum of three integrals of the type,

$$\int u^m e^{-\gamma u} \cos bu \, du = e^{-\gamma u}\left(\frac{1}{\rho} u^m \cos(bu - \phi)\right)$$
$$- \frac{m}{\rho^2} u^{m-1} \cos(bu - 2\phi) + \frac{m(m-1)}{\rho^3} u^{m-2} \cos(bu - 3\phi)$$
$$- \frac{m(m-1)(m-2)}{\rho^4} u^{m-3} \cos(bu - 4\phi) + \cdots, \quad (15)$$

TABLE I. Nine-and nineteen-point roots and weight factors for the Gauss-Legendre quadrature.[7]

Roots (z_i)	Weight factors (W_i)
Nine-point	
0.000 000	0.330 239
± 0.324 253	0.312 347
± 0.613 371	0.260 611
± 0.836 031	0.180 648
± 0.968 160	0.081 274
Nineteen-point	
0.000 000	0.161 054
± 0.160 359	0.158 969
± 0.316 564	0.152 766
± 0.464 571	0.142 607
± 0.600 545	0.128 754
± 0.720 966	0.111 567
± 0.822 715	0.091 490
± 0.903 156	0.069 045
± 0.960 208	0.044 814
± 0.992 407	0.019 462

[This article is copyrighted as indicated in the article. Reuse of AIP content is subject to the terms at: http://scitation.aip.org/termsconditions. Downloaded to] IP: 128.173.126.47 On: Wed, 06 May 2015 21:25:18

TABLE II. Least-squares analysis of two Mo films on (111) Si and one InSb on (111) GaAs.

Sample	$<L>$ (A)	$<\epsilon_{1D}^2>^{1/2}$ $\times 10^2$	$<\epsilon_{1U}^2>^{1/2}$ $\times 10^2$	ϕ/M $\times 10^5$
1 Mo/Si	186	1.37	0.310	6.91
2 Mo/Si	884	1.30	0.143	4.60
3 InSb/GaAs	1337	0.42	0.042	12.8

where $\rho = (b^2 + \gamma^2)^{1/2}$, $\cos\phi = -\gamma/\rho$, $\phi = \pi - \tan^{-1}(b/\gamma)$. This result is given by

$$\frac{P_1'(h_3^0)}{2N_3Y_0} = \frac{1}{(2\pi h_3^0)^2 + \gamma^2} \times \left(\gamma + \frac{(2\pi h_3^0)^2 - \gamma^2 + \frac{8}{9}\cos[4\tan^{-1}(2\pi h_3^0/\gamma)]}{(2\pi h_3^0)^2 + \gamma^2} \right) - \mathrm{FLC}$$

and

$$\mathrm{FLC} = \frac{e^{-(3/2)\gamma}}{[(2\pi h_3^0)^2 + \gamma^2]^{3/2}} \left(\frac{4}{3}\cos[3\pi h_3^0 + 3\tan^{-1}(2\pi h_3^0/\gamma)] \right) + \frac{8}{9}\frac{\cos[3\pi h_3^0 + 4\tan^{-1}(2\pi h_3^0/\gamma)]}{[(2\pi h_3^0)^2 + \gamma^2]^{1/2}}. \tag{16}$$

The first term in Eq. (16) can be obtained from Eq. (14) by allowing the upper limit to go to infinity. A finite limit introduces an additional term given by FLC. This finite limit correction, of course, results from the 3/2 cutoff point of the particles size coefficient given in Eq. (6a). If the term $e^{-\gamma u}$ were to converge to zero before A_n^S, the FLC can be neglected.

Although the complete solution has not yet been obtained, Eq. (16) can be used to analyze cold-worked metals under certain restricted conditions. First, the specimen broadening must be due only to small particle size and dislocation originated strain ($r = -\frac{1}{2}$). Second, the instrumental broadening must either be relatively small or a pure Cauchy function. The latter is approximately attained with a well-focused monochromater that removes the $K_{\alpha 2}$ component of the K_α doublet and ideal diffractometer conditions.

In order to complete the calculation of Eq. (14) with $\beta \neq 0$, it must be recognized that this term originates from a Gaussian function with a half-width determined by $<\epsilon_{1U}^2>$ and a_β^2, i.e.,

$$g_3(h_3^0) = Y_0' \exp[-\pi h_3^{02}/N_3^2(a_\beta^2 + 2\pi <\epsilon_{1U}^2> l^2)], \tag{17}$$

or, that the cosine transform of Eq. (17) gives the original term $e^{-\beta u^2}$ when properly normalized. Equation (17) remains Gaussian after convoluting the Gaussian strain broadening with the Gaussian contribution from instrumental broadening.

Unfortunately, one must resort to a numerical convolution of Eq. (16) with Eq. (17) to obtain the final result. This can be carried out accurately using a nine-point Gauss-Legendre quadrature.[6,7] The required convolution integral is

$$P_2'(h_3^0) = Y_0'' \int_{-b}^{b} g_3(x) P_1'(h_3^0 - x)dx, \tag{18}$$

where Y_0'' is a scaling constant and the limits $\pm b$ are established to encompass most of the area of $g_3(x)$. A typical value that has been used and one which does not introduce a significant termination error is 99.9%. The numerical integration by Gauss-Legendre quadrature is normally carried out with the new variable z that causes the limits to be ± 1,

$$P_2'(h_3^0) = Y_0'' \int_{-1}^{1} g_3(bz) P_1'(h_3^0 - bz)dz,$$

or as a nine-point quadrature,

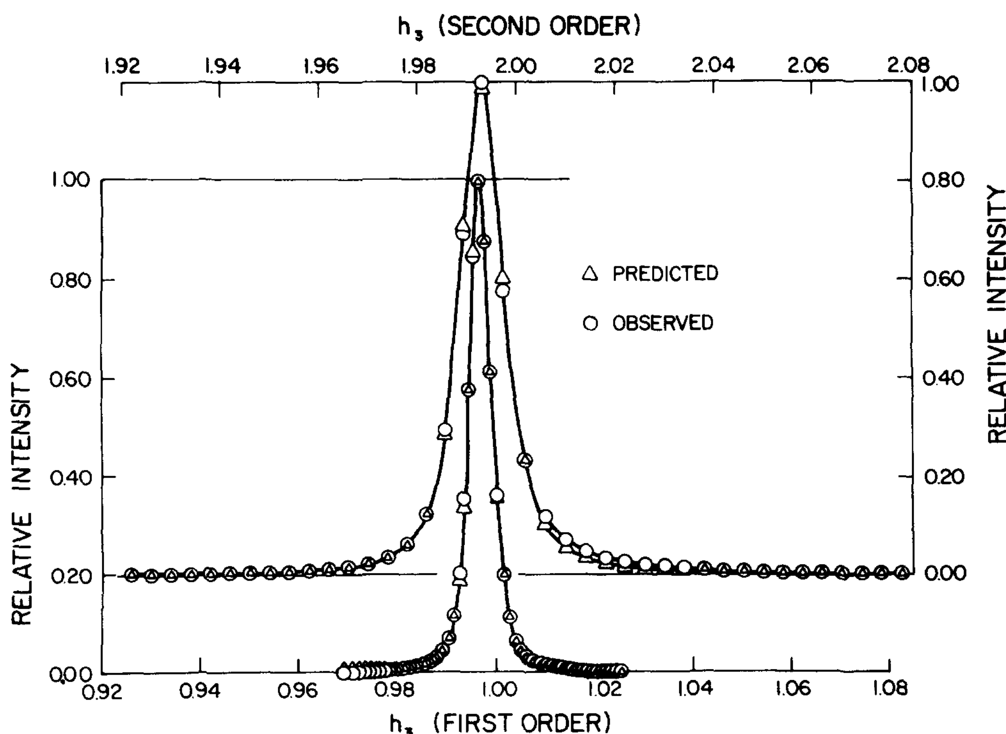

FIG. 1. Fit of Eq. (19) to data obtained from Mo/Si sample 2 for two orders. The fit for every third point is illustrated.

[This article is copyrighted as indicated in the article. Reuse of AIP content is subject to the terms at: http://scitation.aip.org/termsconditions. Downloaded to] IP: 128.173.126.47 On: Wed, 06 May 2015 21:25:18

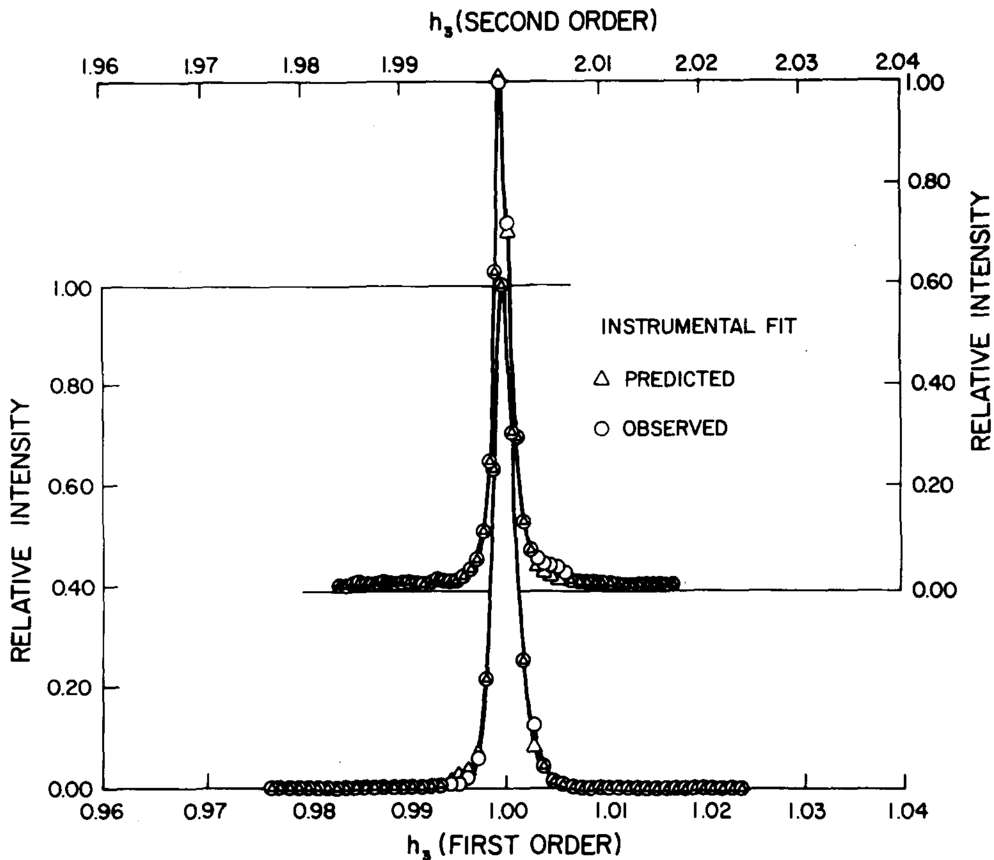

FIG. 2. Instrumental fit using Eq. (20) for two orders from a Mo powder. The fit for every third data point is illustrated.

$$P_2'(h_3^0) = Y_0'' \sum_{i=1}^{9} W_i \left[g_3(bz_i) P_1'(h_3^0 - bz_i) \right]. \quad (19)$$

The weighting factors W_i and roots z_i are given in Table I for nine-and nineteen-point quadratures.

Special considerations must be given to the determination of the instrumental parameters a_γ and a_β. In order to reduce computer time, the instrumental function was obtained by convoluting Eqs. (8) and (10) directly using a nineteen-point Gauss-Leqendre quadrature. This is given by

$$P_3'(h_3^0) = Y_0'' \sum_{i=1}^{19} W_i \left[\left(1 + \frac{(h_3^0 - bz_i)^2}{a_\gamma^2} \right)^{-1} e^{-\pi b^2 z_i^2 / a_\beta^2} \right]. \quad (20)$$

Trial and error fitting with a different number of points indicated that 19 points is adequate to fit this sharp function. The weighting factors and roots are given in Table I. Although a greater number of points are required to fit the instrumental function, the overall least-squares fitting time is less than the time required to do a least-squares fitting with Eq. (19). This, of course, is expected because of the complexity of the latter equation.

SEVERAL EXAMPLES OF LINE SHAPE FITTING

All of the following examples of line shape fitting deal with sputtered films. Two of the data sets were obtained from samples containing Mo films on (111)-oriented Si single-crystal substrates prepared under different conditions. A third sample contained a (111)-oriented single crystal InSb film on a (111) GaAs crystal. The greatest line broadening was obtained from one of the Mo films while the smallest was obtained from the InSb film. All data were collected with a diffracted beam quartz monochromator, a fine focus Siemens diffraction tube, and a 0.05-mm receiver slit. The monochromator was set to reject the $K_{\alpha 2}$ line.

Table II illustrates the results of a least-squares analysis of all three samples as performed on an IBM 370 system. These results include the average x-ray particle size ($\langle L \rangle$), two strain parameters, and the sum of squares deviation per point for fitting two orders (ϕ/M). The Mo results made use of the (110) and (220) reflections while the InSb data used the (111) and (444). Figure 1 illustrates the fit to the actual data using Eq. (19) while Fig. 2 illustrates the fit for a pair of

TABLE III. Curve fitting with incomplete profiles of equally spaced points—No background truncation (a) and lower one-half of profile (b). Sample 2 Mo/Si.

Data set	M	$\langle L \rangle$ (A)	$\langle \epsilon_{1D}^2 \rangle^{1/2}$ $\times 10^2$	$\langle \epsilon_{1U}^2 \rangle^{1/2}$ $\times 10^2$	ϕ/M $\times 10^5$
(a) 20 FWHM	302	884	1.30	0.143	4.60
(b) ½ of points (lower 2Θ)	154	1001	1.29	0.154	3.26
(c) 50% back. t.	154	867	1.31	0.141	7.89
(d) 75% back. t.	74	730	1.35	0.130	9.25
(e) 90% back. t.	30	608	1.39	0.115	4.94

[This article is copyrighted as indicated in the article. Reuse of AIP content is subject to the terms at: http://scitation.aip.org/termsconditions. Downloaded to] IP: 128.173.126.47 On: Wed, 06 May 2015 21:25:18

instrumental curves using Eq. (20). The small deviation on the high side of the second order peak is due to incomplete rejection of the $K_{\alpha 2}$ line. A computer time of 222 sec was required to obtain a best fit for sample 2 and this took 12 separate calculations for each pair of profiles to arrive at the minimum sum of the squares with 302 data points. Each pair of reflections requires about 19 sec of computer time to generate profiles for a given set of parameters when 302 data points are used.

In many applications, one cannot obtain reliable data for an entire profile because of overlapping peaks. Sample 2 was reanalyzed with various subsets of data points deleted from each peak within a pair. These results are illustrated in Table III. The first entry contains data over a 2Θ range of twenty times the full width at the half maximum (20 FWHM) arranged with the peak approximately at the center of each interval. The same number of points were selected to represent each peak and all points were equidistant on the h_3 scale. If only the points on the low side of each peak are used, one still finds good agreement with the full analysis. The rather large particle size of ~ 900 A, which was found in this sample, is expected to be subject to error because of the small broadening associated with this size. The effect of background truncations of 50, 75, and 90% is also given. It would appear that this analysis still gives a very reasonable particle size with a 50% truncation of background. However, with 75 and 90% truncations, the particle size gives increasingly obvious deviations. It is surprising to find that the strain parameters remain nearly constant even with considerable truncation. These results indicate that reliable particle size and strain information can be obtained from incomplete profiles when two orders are used. This agreement cannot to be expected when using the conventional Warren-Averbach line shape analysis.

In order to relate the sensitivity of ϕ/M to variations of $\langle L \rangle$, $\langle \epsilon_{1D}^2 \rangle$, and $\langle \epsilon_{1U}^2 \rangle$, these were varied holding the other two fixed at the minimum (see Figs. 3, 4, and 5, respectively). Figure 3 illustrates this response curve to variations in $\langle L \rangle$. Also illustrated are the truncation points b, c, d,

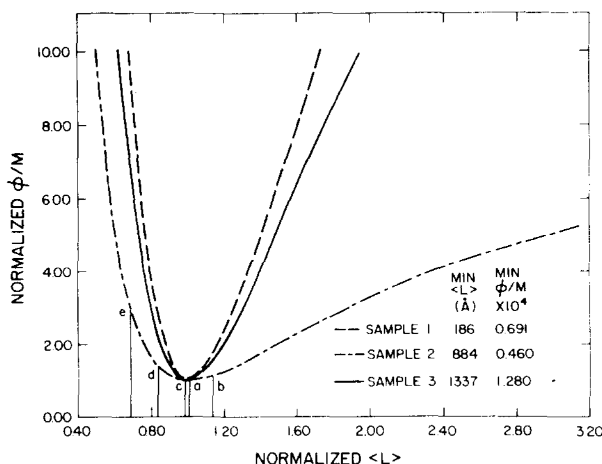

FIG. 3. Misfit error $\phi/M/(\phi/M)_{\min}$ vs normalized $\langle L \rangle$, $\langle L \rangle / \langle L \rangle_{\text{opt}}$, for three samples, where $\langle L \rangle = \langle d \rangle N_3$. Both strain parameters are held at the optimum values as given in Table II.

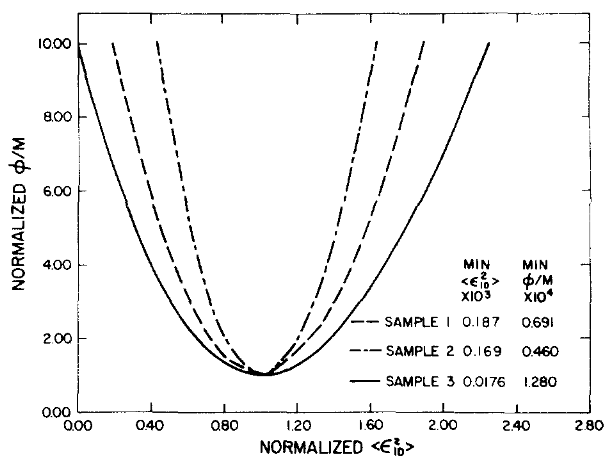

FIG. 4. Misfit error vs normalized $\langle \epsilon_{1D}^2 \rangle$, $\langle \epsilon_{1D}^2 \rangle / \langle \epsilon_{1D}^2 \rangle_{\text{opt}}$, for three samples. $\langle L \rangle$ and $\langle \epsilon_{1U}^2 \rangle$ are held at the optimum values given in Table II.

and e corresponding to the $\langle L \rangle$ values given in Table III (sample 2). It can be seen that all of these points are within $\phi/M < 10^{-4}$. Plots within this range would appear to give good visual fits with the data. An examination of Figs. 3, 4, and 5 show that sample 2 has a relatively broad response curve for particle size variations and sharp curves for the strain parameters. This is because the major contribution to the line broadening is due to strain and not particle size. Sample 3 has the smallest broadening contribution from strain and is primarily broadened by particle size. As one might expect, the particle size response curve is the sharpest. These curves are useful for evaluating the various contributions to the line broadening and therefore the degree of confidence that may be associated with the parameters defining the minimum points. Data from sample 1 is influenced by all three types of broadening giving three relatively sharp response curves.

Thus far all of the data have been analyzed as multiple order pairs. It is tempting to examine the misfit generated when only one peak is used for the analysis. If the broadening associated with each effect is sufficiently distinctive, one might expect to extract all three parameters from one peak.

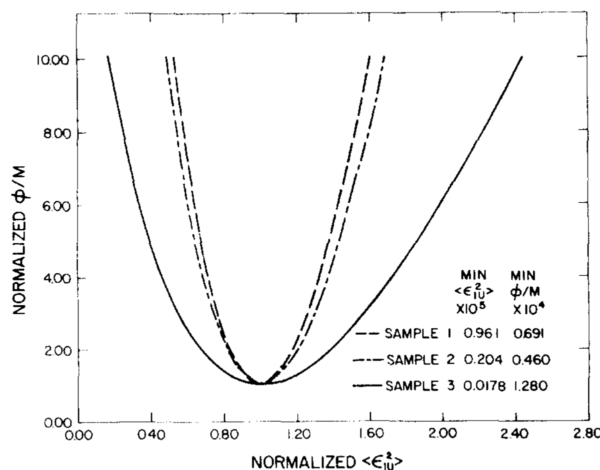

FIG. 5. Misfit error vs normalized $\langle \epsilon_{1U}^2 \rangle$, $\langle \epsilon_{1U}^2 \rangle / \epsilon_{1U\,\text{opt}}^2$, for three samples. $\langle L \rangle$ and $\langle \epsilon_{1D}^2 \rangle$ are held at the optimum values given in Table II.

[This article is copyrighted as indicated in the article. Reuse of AIP content is subject to the terms at: http://scitation.aip.org/termsconditions. Downloaded to] IP: 128.173.126.47 On: Wed, 06 May 2015 21:25:18

TABLE IV. ϕ/M minima for Sample 2 Mo/Si using single peak and two peak analyses.

Starting N_3	N_3	$<L>$	$<\epsilon_{1D}^2>^{1/2}\times 10^2$	$<\epsilon_{1U}^2>^{1/2}\times 10^2$	$\phi/M\times 10^5$
First order only					
50	302	673	0.78	0.157	3.19
100	335	744	0.86	0.160	3.14
150	356	792	0.92	0.161	3.17
200	390	867	1.04	0.160	3.29
250	528	1174	1.28	0.157	4.01
300	352	783	0.93	0.160	3.16
Second order only					
50	182	406	1.34	0.102	1.99
100	524	1166	1.49	0.113	1.96
150	303	674	1.44	0.109	1.96
200	300	667	1.43	0.110	1.96
250	144	320	1.28	0.091	2.05
300	349	776	1.45	0.112	1.96
Both orders					
50	417	929	1.30	0.144	4.61
100	397	884	1.30	0.143	4.60
150	372	827	1.30	0.140	4.64
200	408	907	1.30	0.144	4.60
250	427	950	1.30	0.145	4.63
300	395	879	1.30	0.143	4.60

Unfortunately, a one peak analysis has not given a unique set. Table IV gives results from separate analyses of the first and second order peaks as well as for an analysis of a pair from sample 2. When the least-squares program is initiated with $<\epsilon_{1D}^2> = 0.5\times 10^{-3}$, $<\epsilon_{1U}^2> = 0.5\times 10^{-5}$, and $N_3 = 50$, 100, 150, 200, 250, and 300 successively, different compositions of parameters usually have low ϕ/M values when only one peak is used. However, for the first order fit alone, both $<L>$ and $<\epsilon_{1D}^2>$ have a large range of values with equally low ϕ/M, while only $<\epsilon_{1U}^2>$ appears to be well defined. For the second order, different initial values of $<L>$ again converge to different points, all of which give low ϕ/M values. When two orders are used, a unique minimum is obtained. The convergence illustrated in Table IV is typical of all paired profiles that have been studied. It is possible that when the total broadening approaches the instrumental broadening, several minimum points will be observed with nearly the same ϕ/M even when a pair is used. This situation has not been observed thus far. Obviously, when this occurs, unique results cannot be obtained from the data. The present data indicates that a single peak analysis of strain and particle size does not give a unique minimum and is to be avoided.

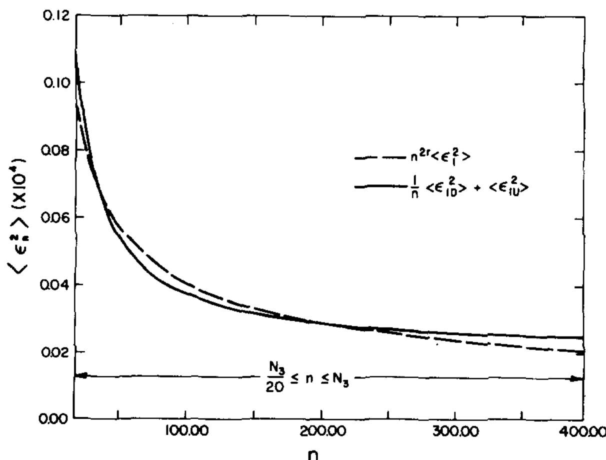

FIG. 6. Intercomparison of the two strain distributions given by Eq. (11) over the range $n/20<n<N_3$ for sample 2.

As a final point, the calculations leading to Eq. (19) are based upon the distribution given by $1/n<\epsilon_{1D}^2> + <\epsilon_{1U}^2>$ rather than $n^{2r}<\epsilon_1^2>$ as given in Eq. (11). In a previous paper,[1] it was pointed out that the profiles are insensitive to the small differences in strain associated with these distributions. This is true because the slowly varying intensity that gives strain information at low n is not usually measurable because of overlapping tails. Likewise, at large n, the strain does not introduce an important effect on the profile because of the small number of pairs of cells that contribute to the intensity profile. The profile is largely shaped by pairs of cells having a separation within the range

$$N_3/20 \leqslant n \leqslant N_3. \quad (21)$$

The strain has been plotted using both distributions within this range for sample 2 (see Fig. 6). The $n^{2r}<\epsilon_1^2>$ strain distribution has been shown to agree with Warren-Averbach analysis strain data[1] but the data scatter most often exceeds the small oscillation introduced by the two term strain distribution. Consequently, either distribution is acceptable. In either case, the nonuniform strain $<\epsilon_n^2>$ should not be interpreted out of the range given by Eq. (21). The parameters $<\epsilon_1^2>$, $<\epsilon_{1D}^2>$, and $<\epsilon_{1U}^2>$ only have meaning when used to calculate $<\epsilon_n^2>$ over the designated range.

ACKNOWLEDGMENTS

Funding for this study was made available by National Science Foundation Grant No. DMR75-17201. The authors are grateful to Satish Rao for providing the data associated with sample 3 in this study.

[1]T. Adler and C. R. Houska, J. Appl. Phys. **50**, 3282 (1979).
[2]B. E. Warren, Prog. Met. Phys. **8**, 147 (1959).
[3]R. L. Rothman and J. B. Cohen, *Advances in X-Ray Analysis*, edited by C.

[This article is copyrighted as indicated in the article. Reuse of AIP content is subject to the terms at: http://scitation.aip.org/termsconditions. Downloaded to] IP: 128.173.126.47 On: Wed, 06 May 2015 21:25:18

S. Barrett, J. B. Newkirk, and G. R. Mallett (Plenum, New York, 1969) Vol. 12.
[4]T. Adler and C. R. Houska, J. Appl. Phys. **50**, 3288 (1979).
[5]A. Guinier, *X-Ray Diffraction* (Freeman, San Francisco, 1963).
[6]B. Carnahan, H. A. Luther, and J. O. Wilkes, *Applied Numerical Methods* (Wiley, New York, 1969).
[7]A. H. Stroud and D. Secrest, *Gaussian Quadrature Formulas* (Prentice-Hall, New Jersey, 1966).

[This article is copyrighted as indicated in the article. Reuse of AIP content is subject to the terms at: http://scitation.aip.org/termsconditions. Downloaded to] IP: 128.173.126.47 On: Wed, 06 May 2015 21:25:18